Jia *et al.*
Egyptian Journal of Medical Human Genetics (2023) 24:77
https://doi.org/10.1186/s43042-023-00457-3

Egyptian Journal of Medical Human Genetics

RESEARCH

Open Access

Identification of the cuproptosis-related ceRNA network and risk model in acute ischemic stroke by integrated bioinformatics analysis

Fang Jia[1], Bingchang Zhang[1], Chongfei Li[1], Weijie Yu[1], Zhangyu Li[1] and Zhanxiang Wang[1*]

Abstract

Background Acute ischemic stroke (AIS) is one of the leading contributors to death and disability in adults. And cuproptosis is a novel type of cell death. Yet, its role in AIS is still unknown.

Methods The mRNA, miRNA, and circRNA expression data were downloaded from the Gene Expression Omnibus database. We explored differentially expressed circRNAs (DEcircRNAs), microRNAs (DEmiRNAs), and cuproptosis-related genes (DECuRGs) after AIS. With the target prediction tools, we constructed a cuproptosis-related competitive endogenous RNA (ceRNA) network mediated by circRNAs in AIS. Afterward, functional enrichment analysis, cytoHubba plugin, protein–protein interaction, weighted gene co-expression network analysis, and unsupervised clustering analysis were performed to determine the critical genes and relevant pathways. Machine learning techniques were used to identify the optimal risk model. The CIBERSORT was applied to explore the immune-infiltrating characteristics in AIS samples. Finally, two independent datasets were employed to verify the predictive value of the risk model.

Results Altogether, 26 DECuRGs were identified in this study. Enrichment analysis revealed that they participated in the reactive oxygen metabolism, inflammatory responses, and corresponding cuproptosis-related biological processes. Of the DECuRGs, *MTF1* and *UBE2D2* were included in the ceRNA network, comprising three circRNA-miRNA and two miRNA-mRNA interaction pairs. Hub gene analysis determined the hub regulatory axis in the process of cuproptosis, namely, *MTF1-miR-765-circ_0040760/0068531*. We finally constructed a 5-gene risk model (*C10orf32*, *NUCB1*, *AX748267*, *MRPL28*, and *PPP1R15A*) by multiple analyses, which was validated by two independent datasets (AUC = 0.958 and 0.668). Besides, significant differences in immune cell infiltration were observed between AIS patients and normal controls. The levels of neutrophils were correlated with most of the DECuRGs. The ceRNA axis identified in this study was also associated with the immune microenvironment of AIS patients.

Conclusion The findings revealed that cuproptosis might be associated with AIS and that the key nodes, including the regulatory axes, might exert critical roles in the process of AIS. The risk model provided new insights into the early diagnosis and treatment of AIS.

Keywords Acute ischemic stroke, Cuproptosis, ceRNA network, Machine learning, Immune infiltration, Risk model

*Correspondence:
Zhanxiang Wang
wangzx@xmu.edu.cn
Full list of author information is available at the end of the article

Introduction

Based on the latest statistics from the World Health Organization, ischemic stroke is the leading contributor to permanent disability in adults and ranks second among the significant causes of death worldwide [1]. Of note, acute ischemic stroke (AIS) due to embolism or artery thrombosis constitutes approximately 85–90% of all stroke cases [2]. Cerebral ischemia provokes a series of pathological events, including intracranial hemorrhage, blood–brain barrier (BBB) disruption, irreversible neuronal death, and angioedema [3]. Despite advances in understanding the pathology of cerebral ischemia, only a few AIS patients benefit from thrombolytic therapy nowadays due to the narrow "time window" [4]. Therefore, exploring the novel molecular mechanism of AIS and screening potential biomarkers for early AIS diagnosis have been top priorities.

Proper levels of copper are indispensable as a catalytic cofactor for primary enzymes participating in the modulation of oxygen transport, energy conversion, and oxidative intracellular metabolism. Although copper serves a fundamental role in many biosynthetic processes [5], it is controversial that copper imbalance features prominently in angiogenesis, oxidative stress, and deficiency of energy metabolism, suggesting its potential in exploring novel therapies for ischemic stroke [6, 7]. Cuproptosis, identified by a study in *Science*, is a novel form of programmed cell death different from pyroptosis, apoptosis, ferroptosis, and necroptosis [8]. The copper-induced cell death is closely related to the enzymatic function of protein-lipid acylation in the tricarboxylic acid (TCA) cycle. Possible mechanisms of cuproptosis may involve mitochondrial stress, abnormal copper metabolism, and some key enzymes (e.g., *FDX1*) [9]. Although cuproptosis was initially widely applied in cancer research, increasing studies have shown that it is also linked to neurological diseases such as Wilson's disease, Alzheimer's disease, and traumatic brain injury [10–12]. Recent studies found that plasma copper was linked to a higher risk of AIS and that excess copper ions in drinking water could be a risk factor for stroke [13]. So far, a growing number of studies have centered on identifying biomarkers of cuproptosis at multiple levels, ranging from morphology, biochemistry, and genetics [14]. Huuskonen et al. [15] found that the copper complex CuII might be a strong candidate for treating AIS with potential inflammation-modulating capacity. Preliminary evidence suggested that aberrant Cu/Se and Cu/Zn molar ratios could be important indicators of nutritional status and oxidative stress levels in AIS patients [16]. Nevertheless, exploring the reliable biomarkers and intrinsic regulatory axes related to cuproptosis in AIS remains a tremendous challenge.

Non-coding RNAs mainly include circular RNAs (circRNAs), long non-coding RNAs (lncRNAs), and microRNAs (miRNAs), which modulate protein coding via multiple mechanisms. This is essential in acute inflammation and pathophysiologic recovery after AIS [17, 18]. The competing endogenous RNA (ceRNA) theory suggests that circRNAs have miRNA binding sites and could compete against mRNA-bound miRNAs to establish ceRNA networks, thus suppressing the regulation of target genes by miRNAs. For example, circSCMH1, a ceRNA for MeCP2, was found to release repression of MeCP2 target gene transcription, inhibit peripheral immune cell infiltration and glial activation, enhance neuronal plasticity, and improve cerebral recovery after stroke in both monkeys and mice [19]. A previous study revealed that circHIPK3 could modulate stroke-induced mitochondrial dysfunction and apoptosis in mice via SIRT1/CDK5R1 sponging miR-148b-3p [20]. However, the specific mechanism of ceRNA in AIS remains complicated.

Neuroinflammation is one of the driving causes of the pathophysiological process of AIS [21]. During brain tissue apoptosis, necrosis, or injury, non-coding RNAs are released from immune, neuronal cells, and other mesenchyme mainly along with extracellular vesicles and may transit to targeted cells to induce gene translation and transcription [22]. Previous research has emphasized the critical role of the mRNAs in AIS. However, there are no reports on the cuproptosis-related ceRNA network involved in the neuroinflammation of AIS. In this work, we intended to explore the role of cuproptosis from the perspectives of inflammation and ceRNA in AIS and to provide a novel insight into the pathogenesis and diagnosis of AIS.

Methods and materials

Dataset collection and pre-processing

First, we downloaded the raw mRNA, miRNA, and circRNA expression profiles from the online GEO database (www.ncbi.nlm.nih.gov/geo). We used "ischemic stroke" as a keyword and restricted "Homo sapiens" and "series." The inclusion criteria were as below: (1) a minimum of three people in each group, same race; (2) the samples contained a group of AIS patients and healthy controls without stroke aged 18 years or older; (3) admission within 24 h of onset; (4) with expression data of plasma or whole blood. The discovery dataset GSE58294, which included mRNA expression matrices of 23 normal controls and 69 AIS samples, was used to construct the ceRNA network. In contrast, GSE16561 and GSE22255 mRNA datasets were used as the validation datasets.

Table 1 The specific information of datasets in this study

Dataset	Platform	Normal samples	AIS samples	Type
GSE195442	GPL31275 (Agilent-085499_SBC human ceRNA microarray)	10	10	Circular RNAs (plasma)
GSE86291	GPL18402 (Agilent-046064 Unrestricted_Human_miRNA_V19.0_Microarray)	4	7	MicroRNAs (plasma)
GSE58294	GPL570 (Affymetrix Human Genome U133 Plus 2.0 Array)	23	69	Messenger RNAs (whole blood)
GSE16561	GPL6883 (Illumina HumanRef-8 v3.0 expression beadchip)	24	39	Messenger RNAs (whole blood)
GSE22255	GPL570 (Affymetrix Human Genome U133 Plus 2.0 Array)	20	20	Messenger RNAs (whole blood)

AIS, Acute ischemic stroke

Specific information about these datasets is presented in Table 1. The original data were first modified into an expression matrix and normalized with the "limma" package [23]. Afterward, batch effects were removed by the "sva" R package [24]. Additionally, 46 cuproptosis-related genes (CuRGs), listed in Additional file 1: Table S1, were acquired based on previous studies [8].

Detection of DEGs and DECuRGs

The "limma" and "edgeR" packages were applied to determine the differential expression of miRNAs, circRNAs, and mRNAs between AIS samples and normal controls, with the criteria set to $|\log_2$fold change (FC)$| \geq 1.0$, 1.0, 0.5, respectively, false discovery rate (FDR) < 0.05 [25]. We included the differentially expressed mRNAs (DEmRNAs) that overlapped with CuRGs as DECuRGs for further analysis. The "pheatmap" and "ggpubr" packages were used for the visualization of volcanoes, heatmaps, and boxplots of DEGs.

Correlation analysis of DECuRGs

To explore the associations between these DECuRGs, we conducted a correlation coefficients analysis on the expression of DECuRGs. *P*-values < 0.05 indicated significant correlations according to the Spearman rank correlation [26]. The results were visualized using the "tidyverse" and "corrplot" R packages.

Construction of ceRNA networks in AIS

To investigate the intrinsic regulatory mechanism of DECuRGs, we established circRNAs-miRNAs-mRNAs ceRNA networks in AIS. At first, miRNAs response elements (MREs) of these DEcircRNAs were identified by the online CSCD database (http://gb.whu.edu.cn/CSCD/). Only interactions supported by conclusive evidence (qPCR, western blotting, and reporter analysis) were included in this study. We then took the overlapping genes between MREs and DEmiRNAs for the following analysis step. Then, target mRNAs of overlapping DEmiRNAs were projected by three databases: miRDB (https://www.mirbase.org/), TargetScan (http://www.targetscan.org/), and miRTarBase (http://mirtarbase.cuhk.edu.cn/php/index.php). To improve the reliability and robustness of the predictions, we cross-analyzed the results obtained from the three databases mentioned above. We matched the DEmRNAs, DECuRGs, and target genes, and only the data of the corresponding miRNAs and the intersecting mRNAs were retained for further study. The Venn diagrams were plotted to visualize the overlapping DEmiRNAs, DEmRNAs, and DECuRGs. Finally, the circRNAs-miRNAs-mRNAs network and DECuRGs-related ceRNA network were established via the Cytoscape software (version 3.8.3).

GeneCards

The GeneCards Database (https://www.genecards.org/) is a center of excellence for the complete annotation of genes. It can merge and extract gene annotation data from more than 80 data repositories, including well-known entities such as BioGPS and GTEx [27]. To identify potential links between key nodes in the ceRNA networks and the peripheral blood immune system, we utilized the wealth of information available in the GTEx and BioGPS databases. This was achieved using the online tool GeneCards, which facilitates access to gene expression scores within the blood, allowing for the identity of genes highly correlated with AIS [28].

Functional annotations and pathways analysis

The "Metascape" database [29], Kyoto Encyclopedia of Genes and Genomes (KEGG) [30], and Gene Ontology (GO) analyses based on the "clusterProfiler" package were applied to make a detailed investigation of the biological mechanisms of DECuRGs. GO functional analysis classifies gene functions into three main groups: molecular function (MF), biological process (BP), and cell component (CC). False discovery rate (FDR) < 0.05 was defined as a criterion for statistical significance.

Construction of a PPI network and selection of key DECuRGs

To explore the functional associations between these DECuRGs, the STRING online database (https://string-db.org/) was applied to estimate interactions among the above DECuRGs [31]. Only genes with an interaction score above 0.700 (high confidence) were selected for the PPI network. The results were finally visualized with the Cytoscape software (version 3.8.3). We then applied the topology MCC and DMNC algorithms in the cytoHubba plugin to determine the top 10 genes (Table 2) in the PPI network.

Consensus clustering for AIS samples

To comprehensively understand the role of cuproptosis in AIS, we conducted unsupervised clustering, using the k-means algorithm, to classify 69 AIS samples into distinct molecular groups based on the expression matrix of the ten key DECuRGs mentioned above [32]. The number of potential clusters (k) was between 2 and 9 to avoid generating too many useless clusters, and the most suitable number of clusters was evaluated by a combination of consistency clustering score (>0.9), principal component analysis (PCA), and cumulative distribution function (CDF) curves.

Immune infiltration characteristics

CIBERSORT is a deconvolution technique for estimating the composition of immune infiltrating cells in samples based on RNA sequence data [33]. We investigated the relative abundances of immune infiltrating cells according to the transcription profiles. The percentage of all immune infiltrating cells in each sample sums to 1. To further investigate the associations between AIS-related immune infiltrating cells and cuproptosis-related genes in the peripheral blood, we conducted the Spearman analysis to estimate the coefficients between DECuRGs expression and the proportions of immune cells. A p-value <0.05 meant a significant correlation. We also explored the immune characteristics in different cuproptosis-related molecular groups. The final results were visualized using the "corrplot" and "ggpubr" packages.

Gene set variation analysis (GSVA)

GSVA was conducted using the "GSEABase" and "GSVA" packages to clarify the variations in the set of enriched genes between different molecular groups. The gene sets were analyzed using the "c2.cp.kegg.symbols.gmt" file from the online MSigDB database. Using the "limma" R package, we compared the groups' differential biological features and pathways by comparing GSVA scores. The t value above two was regarded as statistically significant.

Weighted gene co-expression network analysis (WGCNA)

The clustering of samples was conducted to validate the associations between clinical features and the expression matrix based on the grouping information. Co-expression modules in the GSE58294 dataset were identified using the "WGCNA" package [34]. Soft power values were filtered by the WGCNA algorithm in building the modules. When the independence was 0.9, the appropriate value was identified. We then established the weighted adjacency matrices and converted them to topological overlap matrices (TOM). Correlations between clinical traits and module eigengene were used to assess module-trait associations. Each module was given a randomized color. Gene significance (GS) was the associations among expression profiles and module phenotypes. Module membership (MM) was described as the relationship of each module eigengene and expression profiles. The filtering standards for hub genes were MM ≥ 0.8 and GS ≥ 0.5.

Table 2 Detailed information of the 10 critical DECuRGs

Gene	Full name	Role	|logFC|	*P*-value
DLD	Dihydrolipoamide dehydrogenase	Marker	0.775090	0.008
DLAT	Dihydrolipoamide S-acetyltransferase	Marker	0.609848	0.006
ATP7B	ATPase copper transporting beta	Marker	0.591289	<0.001
SCO1	Synthesis of cytochrome C Oxidase 1	Marker	0.522479	0.046
COX11	Cytochrome c oxidase copper chaperone COX11	Suppressor	0.632915	0.037
SOD1	Superoxide dismutase 1	Suppressor	0.586206	<0.001
SLC31A1	Solute carrier family 31 member 1	Marker	0.706957	<0.001
SCO2	Synthesis of cytochrome C oxidase 2	Marker	0.578579	<0.001
MTF1	Metal regulatory transcription factor 1	Marker	0.801954	<0.001
CCS	Copper chaperone for superoxide dismutase	Suppressor	0.651379	<0.001

DECuRGs differentially expressed cuproptosis-related genes

Construction of the risk model using machine learning techniques

Based on the filtered hub genes, we used the "DALEX" and "caret" packages to construct machine learning models [35]. To enhance the reliability of diagnosing AIS, we compared the prediction performance of four algorithms, namely eXtreme Gradient Boosting (XGB), Random Forest Model (RF), Generalized Linear Model (GLM), and Support Vector Machine Model (SVM). In brief, XGB automatically chooses the optimal number of characteristics out of all collected attributes depending on their weights for predicting a particular outcome [36]. RF is an aggregated machine-learning technique that requires no specific regression model to be specified [37]. SVM is a robust classifier tool widely applied for cancer subtype delineation or genome classification [38]. GLM is an advanced version of the multiple logistic regression model and provides the flexibility to assess the associations between continuous independent features and normally distributed dependent characteristics [39]. The expression profiles of AIS were classified randomly into a test set (30%) and a training set (70%). All four machine learning modules operated at default arguments and were evaluated by five-fold cross-validation. Consequently, the model with the optimal performance was identified, and the top 5 most significant variables were chosen to construct a nomogram. Each predictive gene has a corresponding point. The "total points" represented the risk of AIS. Subsequent calibration curves and decision curve analysis (DCA) were applied to estimate the diagnostic power of this risk model.

External validation

Two independent blood datasets, GSE16561 and GSE22255, were utilized to verify the diagnostic accuracy of our risk model. We then applied the "pROC" package to display the areas below the receiver operating characteristic (ROC) curves. Moreover, we conducted a correlation analysis to explore the associations between the expression levels of these five predictors and age.

Statistics

All graphical work and statistical analyses were processed with the R software (version 4.2.2) and the packages mentioned above. Student's *t*-test examined the differences between the two sets. The Bonferroni method was used to correct p-values when samples were large and multiple comparisons were required. The Spearman correlation analysis was applied to explore the associations, and the Bartlett testing was used to assess the variance homogeneity. Significant differences were considered at $P < 0.05$ for each analysis.

Results

DEGs and dysregulated cuproptosis-related genes

A total of 201 DEcircRNAs were directly identified between AIS samples and healthy controls in the GSE195442 dataset, including 78 downregulated and 123 upregulated circRNAs. Meanwhile, ten downregulated DEmiRNAs were screened in the GSE86291 dataset. Based on the differential analysis of the GSE58294 dataset, 710 DEmRNAs were identified, including 360 upregulated and 350 downregulated mRNAs. We displayed the results in the form of volcano plots in Fig. 1A–C. The heatmaps of DEGs are shown in Fig. 1D–F. Due to the large number of DEmRNAs and DEcircRNAs, we only showed the top 50 most significant genes.

To investigate the functions of cuproptosis-related genes in the pathogenesis of AIS, we comprehensively assessed the expression of 46 CuRGs in the 710 DEmRNAs and identified 26 DECuRGs. The expression levels of these genes were shown in the form of box graphs and heatmaps (Fig. 2A, B). Additionally, we conducted a correlation analysis to investigate whether DECuRGs interacted with each other in the occurrence of AIS. Some gene pairs, like COX11 and MAP2K2, showed a robust antagonistic effect (coefficient = −0.63), while pairs like DLD and DLAT showed a synergistic action (coefficient = 0.71). Moreover, both CD274 and SCO2 were found to be associated with most of the other DECuRGs (Fig. 2C). The correlation network further revealed the close relationship between these DECuRGs (Fig. 2D).

The cuproptosis-related ceRNA network

To increase the confidence of this analysis, we only kept the overlapping interaction pairs of the prediction datasets and constructed a circRNA-mediated ceRNA network using the Cytoscape software. The Venn diagrams showed that 7 of 10 DEmiRNAs in the GSE86291 dataset matched the miRNAs response elements (MREs) in the GSE195442 (Fig. 3A). The prediction of TargetScan, miRDB, and miRTarBase databases showed that 7 DEmiRNAs might combine with 2852 target mRNAs. We then incorporated these 2852 mRNAs with the 710 DEmRNAs and the 26 DECuRGs, retaining 105 overlapped DEmRNAs and only 7 overlapping DECuRGs (Fig. 3B, C). Finally, 59 mRNAs, 6 miRNAs, and 12 circRNAs constituted a competing endogenous RNA network (Fig. 3D). More importantly, *MTF1-hsa-miR-765-hsa_circ_0040760/0068531* and *UBE2D2-hsa-miR-4769-3P-hsa_circ_008-5199* axes were identified as the cuproptosis-related ceRNA complexes (Fig. 3E).

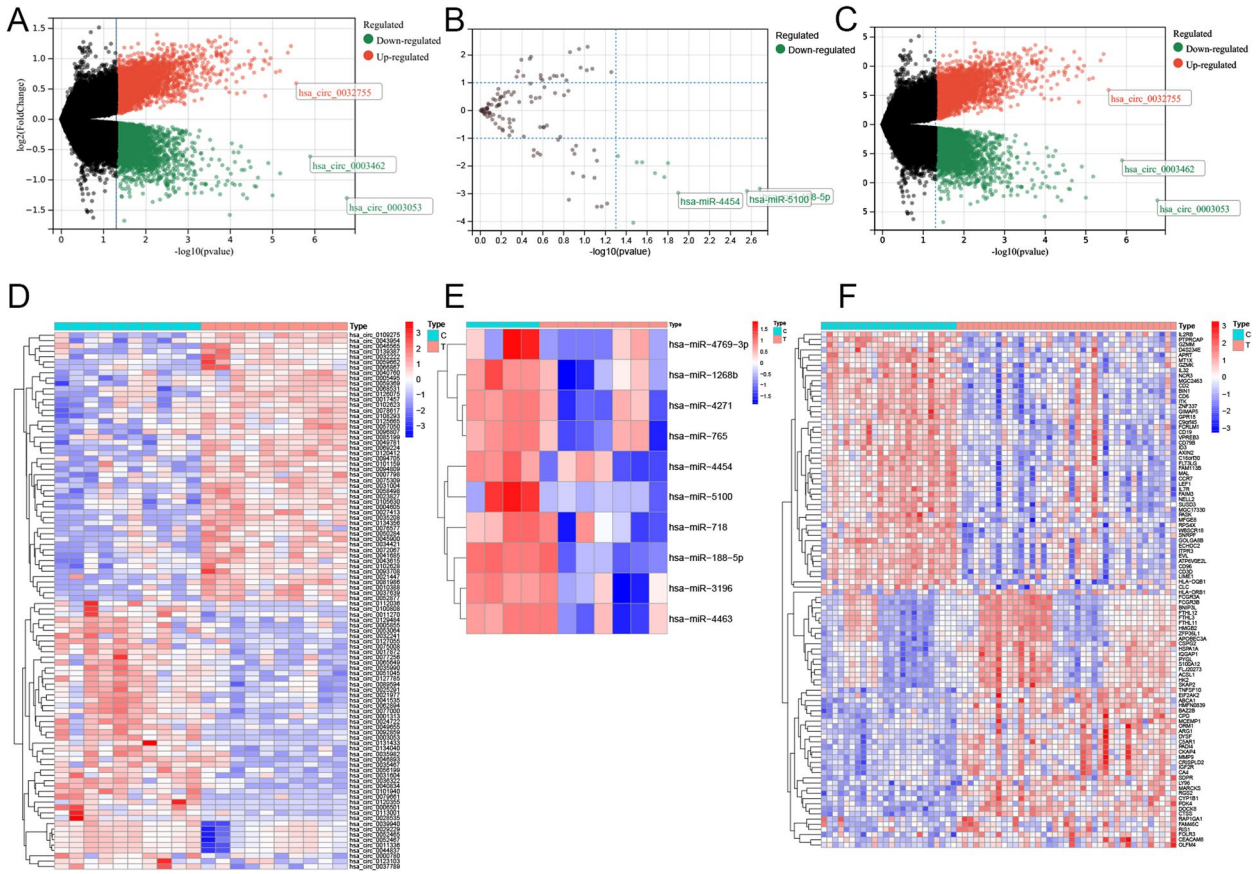

Fig. 1 Differential expression analysis. **A** Volcano map showing the DEcircRNAs in the GSE195422 dataset. **B** Volcanic plot displaying the DEmiRNAs from the GSE86291 dataset. **C** Volcano map exhibiting the DEmRNAs in the GSE58294 dataset; red and blue dots indicate up-and-downregulated genes between AIS samples and normal controls, respectively. Black dots denote genes that are not differentially expressed. Heatmaps for the DEcircRNAs (**D**), DEmiRNAs (**E**), and DEmRNAs (**F**). The color code indicates the gene expression abundance

Exploration of the key nodes

We searched the GeneCard database for key nodes (*MTF1*, *miR-765*, *UBE2D2*, *miR-4769-3P*, and matching circRNAs) to determine their expression in each system. The results showed their high expression levels in the immune system, especially the blood (Additional file 4: Figure S1A–D). GTEx analysis also revealed high bulk tissue gene expressions for these critical nodes in the whole blood (Additional file 5: Figure S2A–D). We concluded that the two ceRNA axes were closely associated with AIS in light of these findings.

Functional enrichment analysis of DECuRGs

We then performed bio-functional and enrichment pathway analysis of DECuRGs using the Metascape database, KEGG, and GO enrichment tools. The Metascape analysis uncovered these genes principally participated in copper homeostasis, cellular response to stimuli, and regulation of pyruvate dehydrogenase (Fig. 4A, B). Similarly, GO results revealed that the DECuRGs were primarily enriched in the cell copper ion homeostasis (BP), mitochondrial matrix (CC), and copper ion binding (MF) (Fig. 4C and Additional file 2: Table S2). KEGG enrichment identified ten markedly enhanced pathways, and the top 3 most significant pathways were the HIF-1 signaling pathway, TCA cycle, and central carbon metabolism in cancer (Fig. 4D and Additional file 3: Table S3). Most of the enriched pathways were consistent with previous studies on stroke and cuproptosis [40, 41], suggesting the reliability of our analysis.

PPI network and key DECuRGs

We first uploaded the 26 DECuRGs into the online STRING database and obtained a complex of 24 co-genes. Afterward, using the Cytoscape software, we established a PPI network carrying 61 cross-talk based on the 24 DECuRGs (Fig. 5A). The cytoHubba was applied to detect key nodes in this network based on the built-in algorithms. We identified a highly connected network consisting of 10 critical DECuRGs (*SLC31A1*, *CCS*,

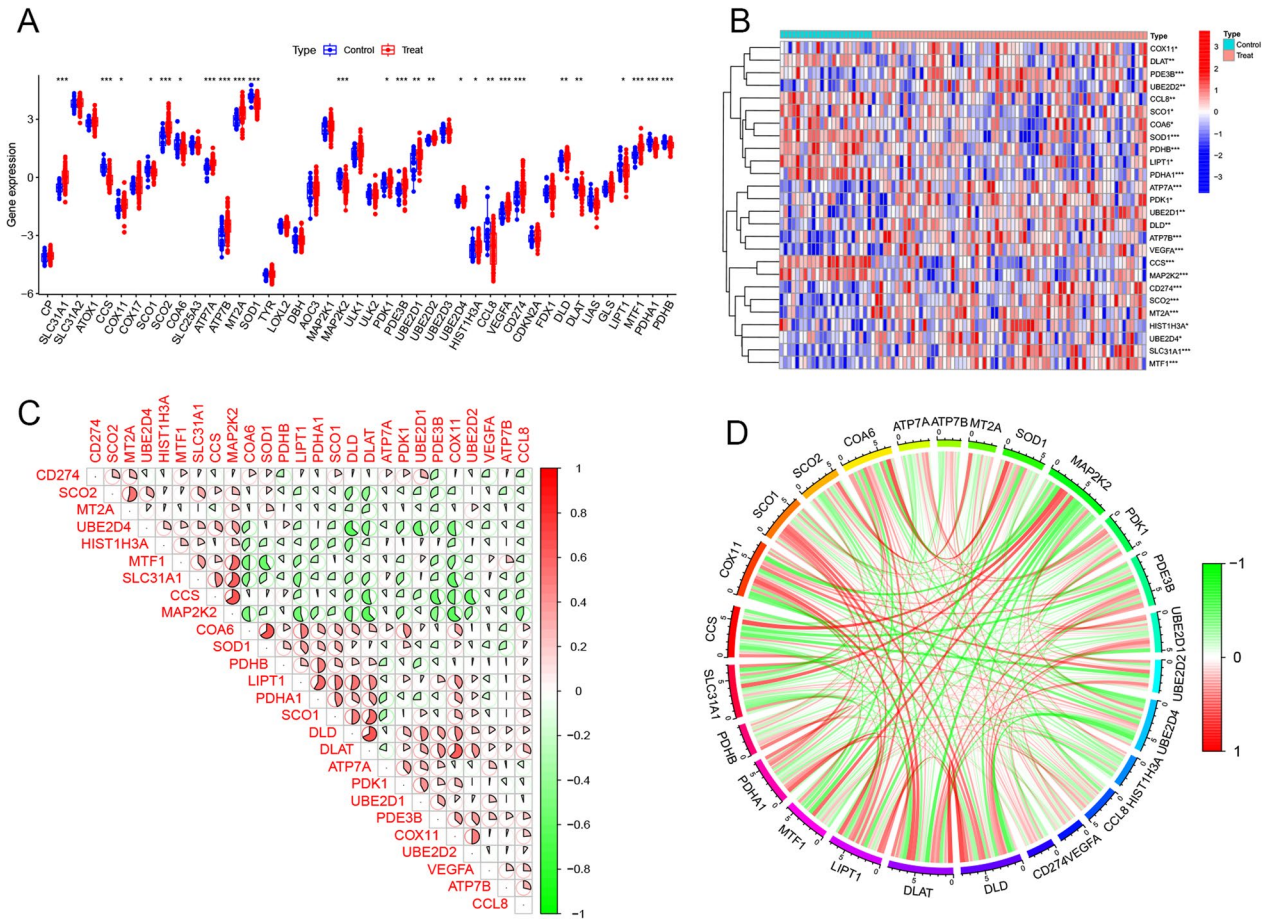

Fig. 2 Dysregulated cuproptosis-related genes in the GSE58294 dataset. **A** Boxplots showing the expression of CuRGs between AIS and normal controls. *$p < 0.05$, **$p < 0.01$, ***$p < 0.001$. **B** Heatmap of the 26 DECuRGs between AIS samples and normal controls. **C** Correlation analysis of the 26 DECuRGs. The size of the pie graph represents the magnitude of the coefficient. Red and green denote positive and negative associations separately. **D** Correlation circular network of the 26 DECuRGs

COX11, *SCO1*, *SCO2*, *MTF1*, *ATP7B*, *SOD1*, *DLD*, and *DLAT*) (Fig. 5B). Subsequent enrichment analyses also indicated that these genes remarkably participated in the cellular copper ion homeostasis (BP), mitochondrial matrix (CC), copper ion binding (MF), and TCA cycle, as were the 26 DECuRGs described above (Fig. 5C–F).

Screening for cuproptosis clusters in AIS

To further investigate the expression patterns of cuproptosis in AIS, we performed an unsupervised cluster analysis to group 69 AIS samples according to the expression landscapes of 10 key DECuRGs. When $k = 2$, the number of clusters was most constant (Fig. 6A). The delta area graph displayed the relevant change in area under CDF curves (Fig. 6B). The maximum difference in the area happened between $k = 2$ and $k = 4$. The minimum consensus index ranged from 0.2 to 0.6 in the CDF curves (Fig. 6C). As presented in Fig. 6D, the clustering consensus score was higher than 0.9 only when the value of k was 2. Furthermore, the results of PCA revealed a distinct difference between the two groups (Fig. 6E). Combining the above results, we eventually divided the 69 AIS samples into two groups, Cluster1 ($N = 40$) and Cluster2 ($N = 29$). We then evaluated the differential expression of 10 DECuRGs across the two groups. The findings showed that Cluster1 exhibited higher COX11, SCO1, ATP7B, DLD, and DLAT expression, while Cluster2 revealed enhanced expressions of *SLC31A1*, *CCS*, and *SCO2* (Fig. 6F, G).

Immune infiltration features in AIS

We obtained the profiles of immune infiltration in AIS samples by analyzing the expression of 21 immune infiltrating cells with the CIBERSORT deconvolution algorithm. The column chart indicated each sample's content of different subtypes (Fig. 7A). The results showed that AIS patients were characterized by higher infiltration ratios of neutrophils, resting dendritic cells, M0

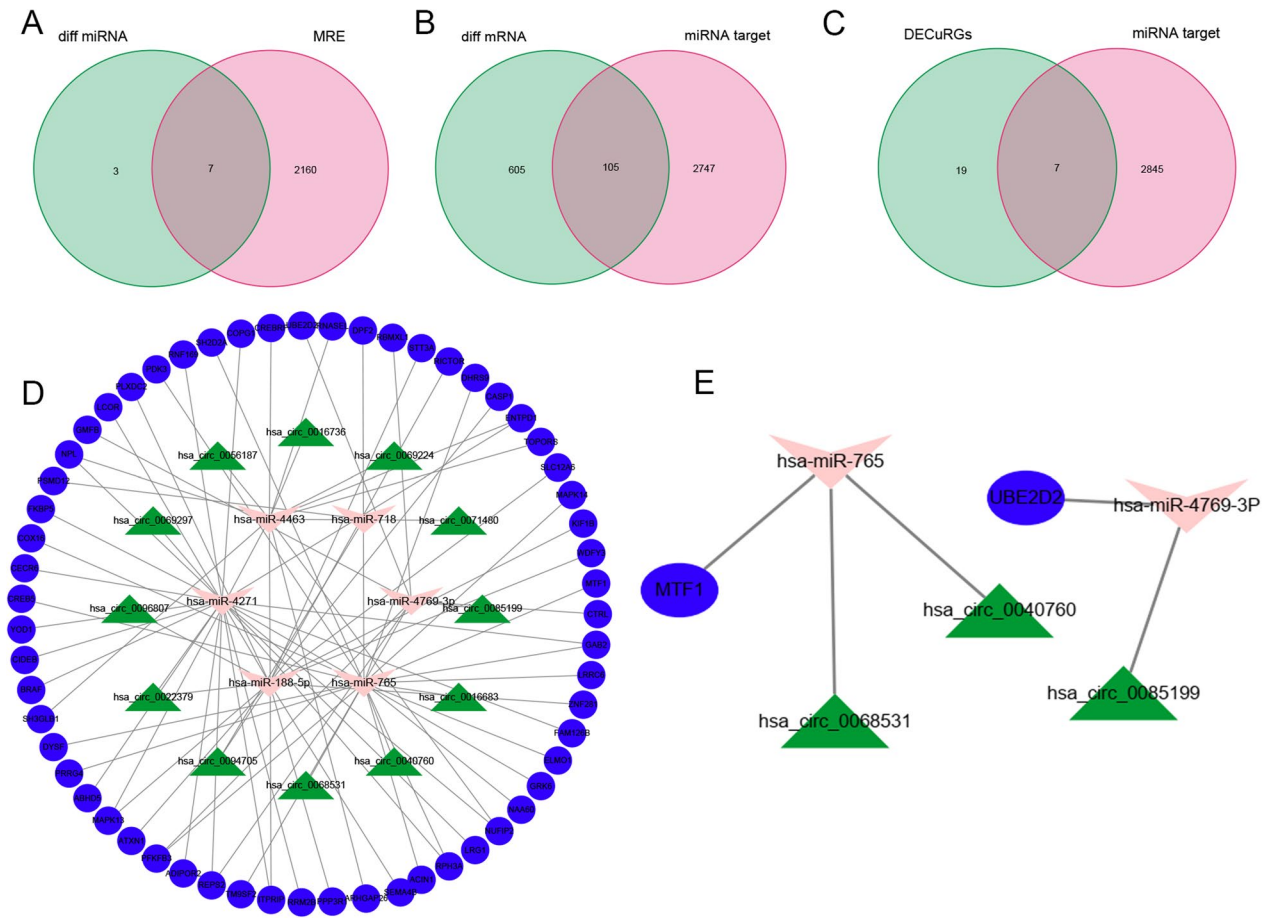

Fig. 3 Construction of the cuproptosis-related ceRNA network. Venn diagrams displaying the seven diff miRNAs found in the intersection of GSE195422 and GSE86291 (**A**), 105 overlapped target diff mRNAs (**B**), seven overlapped genes between the DECuRGs and miRNAs-targeted mRNAs (**C**). **D** The construction of circRNA-mediated ceRNA network, including 12 DEcircRNAs (dark green triangle), 6 DEmiRNAs (light red V), and 59 DEmRNAs (dark blue ellipse). The lines denote their interactions. **E** The construction of cuproptosis-related ceRNA subnetwork via 3 DEcircRNAs, 2 DEmiRNAs, and 2 DECuRGs (*MTF1* and *UBE2D2*)

macrophages, follicular helper T cells, activated memory $CD4^+$ T cells, and monocytes (Fig. 7B), indicating that an altered immune microenvironment could be implicated in the progress of AIS. Moreover, correlation analysis revealed that the levels of neutrophils were correlated with most of the DECuRGs among the 21 immune cell subtypes, suggesting a pivotal role in regulating cuproptosis (Fig. 7C). Interestingly, among the 26 DECuRGs, the expression levels of *MTF1* were most closely related to immune infiltrating cells. *MTF1* and the levels of M0 macrophages presented the most potent synergistic effect (coefficient = 0.64) but showed a distinct antagonistic effect with the levels of resting mast cells (coefficient = −0.52). Combined with the results of ceRNA networks, we speculated that the *MTF1-miR-765-circ_0040760/0068531* axis was the potential cuproptosis-related ceRNA complex with immune infiltration landscapes that could partially capture the microenvironment status in AIS patients.

Furthermore, we investigated the immune characteristics of the two cuproptosis clusters. The results revealed that the variations in the levels of immune-infiltrating cells between Cluster1 and Cluster2 were not as significant (Fig. 7D). Cluster1 displayed higher ratios of naïve B cells, while Cluster2 showed a higher percentage of regulatory T cells (Fig. 7E). In addition, we performed the GSVA to investigate the differences in biological processes in the two groups (Fig. 7F). The results showed that basal transcription factors, protein export, and ubiquitin-mediated proteolysis were upregulated in Cluster2, while vascular smooth muscle contraction and sulfur metabolism were reinforced in Cluster1. Similarly, the discrepancy in immune-related pathways between these two clusters was insignificant.

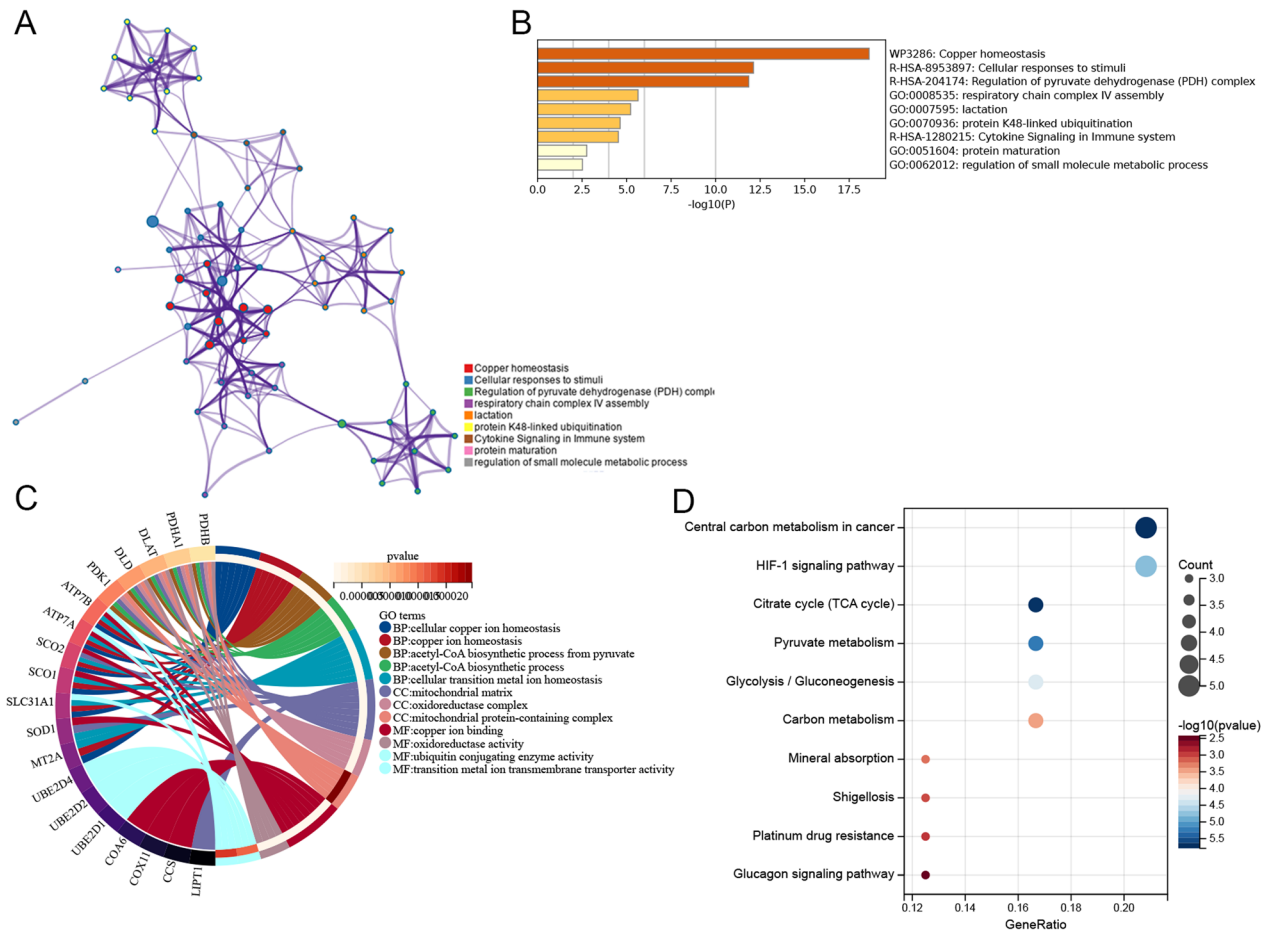

Fig. 4 Functional enrichment analyses of the 26 DECuRGs. **A** Interaction relationship between the enriched terms. **B** Heatmap of the enriched terms. **C** Significant GO enrichment terms for the DECuRGs (MF, molecular function; CC, cellular component; BP, biological process). **D** KEGG enrichment pathway analysis of the DECuRGs

Selection of cluster-specific hub genes

To detect critical gene modules associated with cuproptosis and AIS, we applied the WGCNA to build co-expression blocks and networks between healthy controls and AIS samples. We evaluated the expression variance for each gene in the GSE58294 dataset. The top quartile of genes with the most prominent variations was then selected for further analysis. Cluster analysis of the samples was performed using the "flashClust" R package, and the findings are presented in Fig. 8A. Second, the most suitable power value was determined (Fig. 8B). When the power value of 5 was set, the scale-free degree was up to 0.9, and co-expression modules with higher connectivity degrees were identified. Four co-expression modules of distinct colors were obtained, and interactions of the four modules were analyzed (Fig. 8C, D). Besides, genes from the four modules were used to analyze the adjacency and similarity of module co-expression with clinical traits. Consequently, the turquoise module presented the highest association with AIS, containing 3369 genes (Fig. 8E). Finally, we drew a scatter plot of gene significance (GS) versus module membership (MM) to identify the hub genes related to AIS in the turquoise module (Fig. 8F). We observed a direct positive association between MM and GS and obtained 254 hub genes (Additional file 4: Table S4) by setting the criteria as MM ≥ 0.8 and GS ≥ 0.5.

Machine learning techniques

To screen hub genes with higher diagnostic values, we performed four validated machine learning algorithms (XGB, SVM, GLM, and RF) based on the profiles of 254 hub genes in the AIS training cohort. Consequently, SVM and XGB models exhibited a lower root-mean-square of residual (Fig. 9A, B). The four models' top ten most crucial feature genes were sorted according to the root-mean-square error (Fig. 9C). In addition, we assessed the properties of the machine-learning techniques in the test

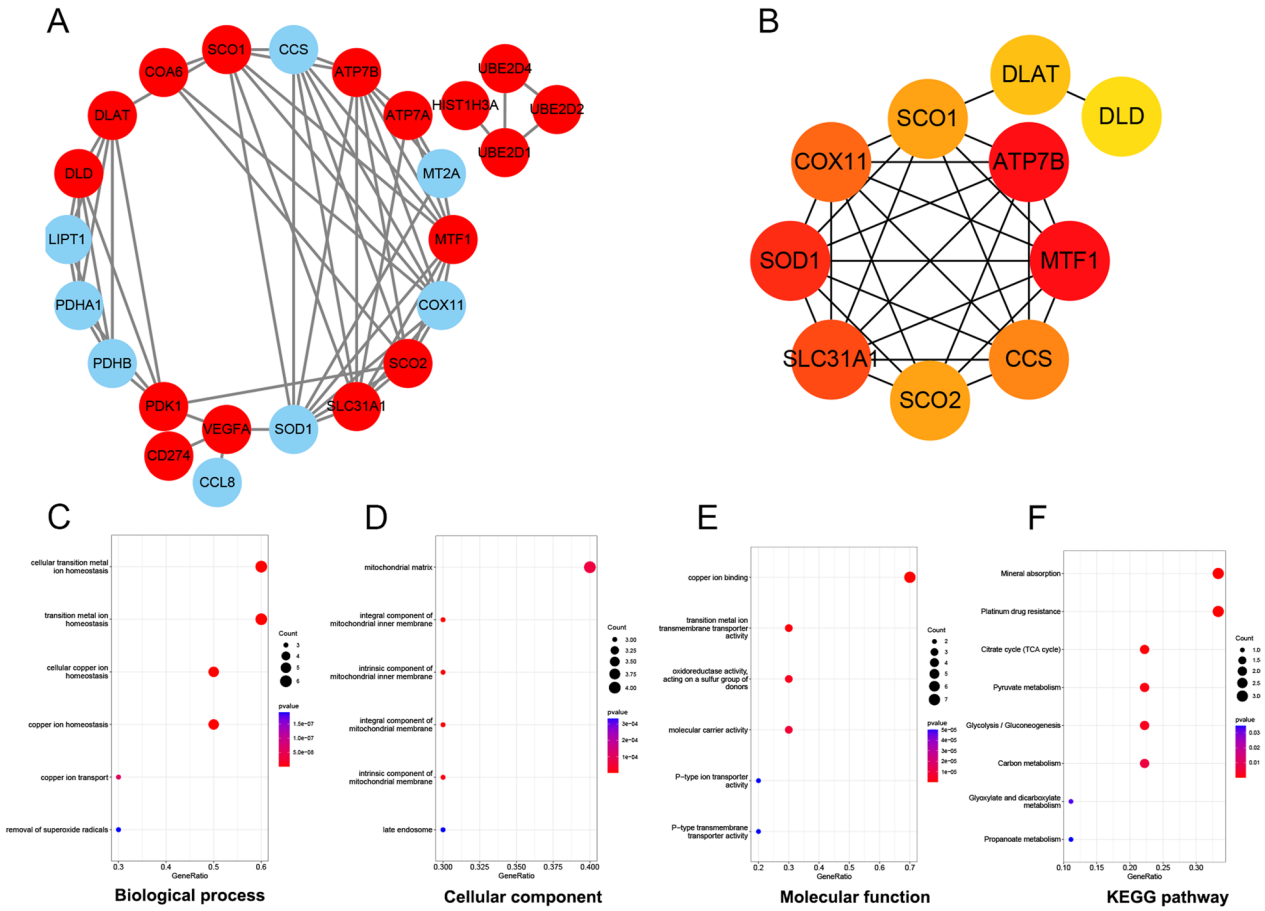

Fig. 5 Protein–protein interaction analysis of the 26 DECuRGs. **A** PPI network comprising of 24 genes. Red dots indicate the upregulated genes, and blue dots denote the downregulated genes. **B** The ten hub genes using the cytoHubba plugin. The darker the red, the higher the degree of connection. GO enrichment analysis of the ten hub genes. **C**–**E** represent the part of biological process, cellular component, and molecular function separately. **F** Significantly enriched KEGG pathway terms

cohort by computing the ROC curves (Fig. 9D). The SVM model performed best with the most significant area under the curves (AUC = 0.956). We then selected the top 5 most essential genes (*C10orf32*, *NUCB1*, *AX748267*, *MRPL28*, and *PPP1R15A*) in the SVM model for further investigation.

Risk model development and validation

The five variables (*C10orf32*, *NUCB1*, *AX748267*, *MRPL28*, and *PPP1R15A*) were used to establish a nomogram model to assess the risk of cuproptosis clustering in the 69 AIS samples (Fig. 10A). Subsequent DCA and calibration curves were applied to evaluate the diagnostic power of the model. The results of DCA indicated that the model was highly accurate and could inform clinical decisions (Fig. 10B). Besides, the calibration curves showed that the actual AIS risk had a tiny error compared to the ideal risk (Fig. 10C). Moreover, we verified the diagnostic model on two independent peripheral blood datasets (including AIS patients and normal controls) using the ROC curve analysis. The AUC values for the GSE16561 and GSE22255 datasets were 0.958 and 0.668, respectively, showing the models' robustness and versatility (Fig. 10D, E). Based on the GSE22255 dataset, we investigated the relationship between the levels of diagnostic genes and age, which was positively correlated with AIS occurrence. We found that only *NUCB1* was negatively and significantly associated with age, R = −0.39, $p = 0.015$ (Fig. 10F–J), implying *NUCB1* was a protective factor for ischemic cerebrovascular diseases.

Using the GSE16561 dataset to verify the hub genes

The five hub genes (*C10orf32*, *NUCB1*, *AX748267*, *MRPL28*, and *PPP1R15A*) were retrieved from the GSE16561 dataset. This dataset contained genetic information of 24 healthy controls and 39 AIS patients. Consequently, the gene *AX748267* was not found in the GSE16561 dataset. We then analyzed the data of the

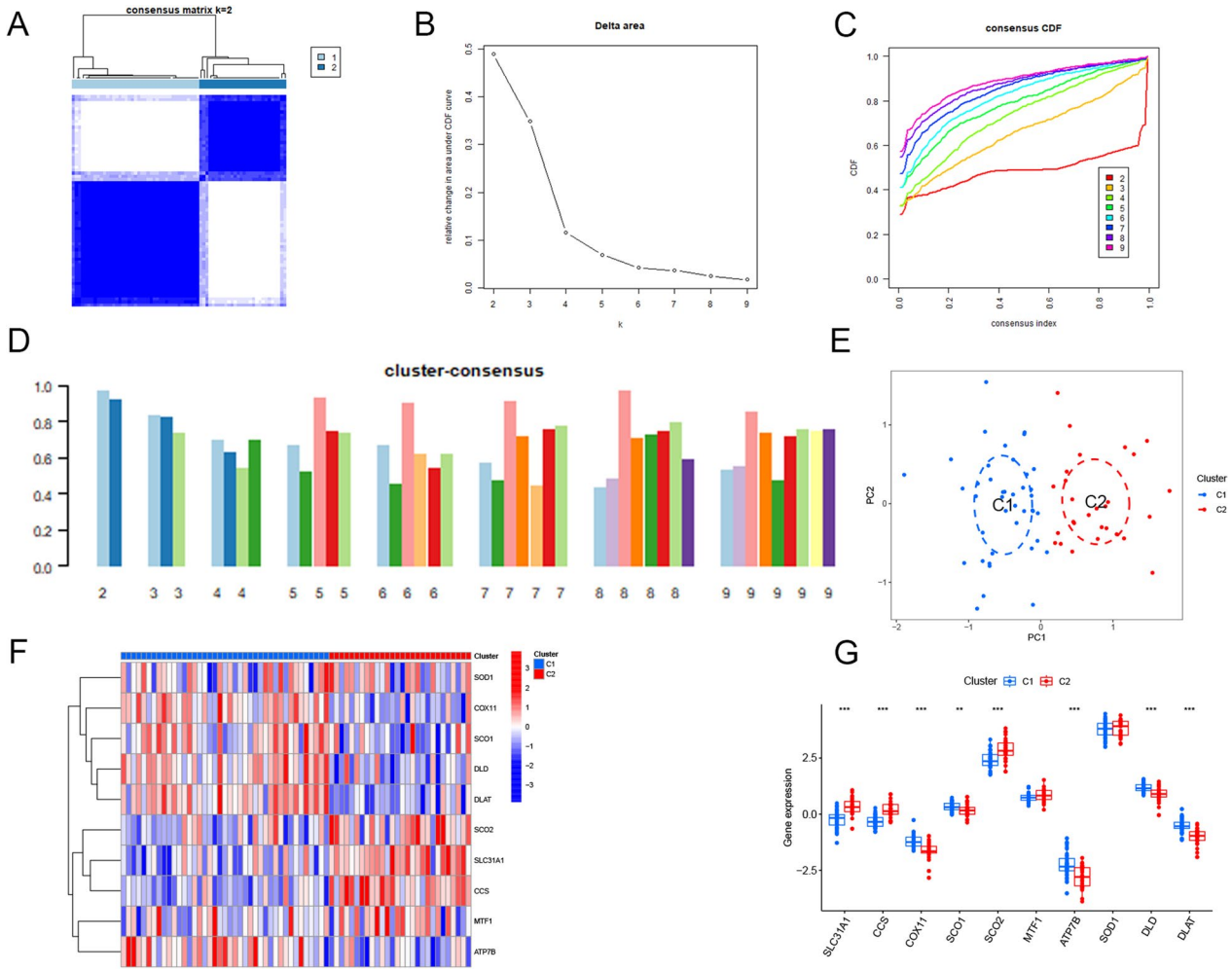

Fig. 6 Exploration of the cuproptosis-related clusters based on the ten key DECuRGs. **A** Consensus clustering matrices at $k=2$. **B** Cumulative distribution function (CDF) relative change in area under the curves. **C** Consensus CDF curves. **D** The cluster-consensus score. **E** The PCA plot. The expression patterns of 10 key DECuRGs in the two clusters were presented as heatmap (**F**) and boxplot (**G**)

other four genes by Student's t-test. Results revealed that the expression of *NUCB1* and *PPP1R15A* was significantly upregulated in the AIS patients (Fig. 11), suggesting the reliability of our analysis.

Discussion

Increasing research supports the involvement of copper-related pathways in the etiopathogenesis of AIS and emphasizes the critical role of the inflammatory environment [15, 42]. Huuskonen et al. found that copper transport in the ischemic brain could regulate the inflammatory response, especially in myeloid cells. The complex Cu II also reduced the ratio of invasive monocytes and preserved endogenous microglia from ischemic injury [15]. In a large European population-based cohort study, ceruloplasmin was the sole inflammation-sensitive protein significantly related to the incidence of atrial fibrillation after adjusting for confounding factors [43]. Nonetheless, the intrinsic mechanism of cuproptosis in AIS remains unclear since this novel form of cell death was first reported [8]. Currently, there is also a lack of validated diagnostic risk models in the clinical utility. Our study focused on the cuproptosis-related genes and overall regulatory ceRNA networks with immune infiltration features and proposed a cuproptosis-related risk model using multiple bioinformatics analyses.

As a novel post-transcriptional regulatory formation, ceRNA has considerable potential for disease study. Several studies suggest that ceRNA regulation networks may be involved in cancer, atherosclerosis, and other non-neoplastic diseases [44–46], which play an essential regulatory role in AIS. In this work, we systematically analyzed the expression profiling of mRNAs, miRNAs, and circRNAs between healthy controls and

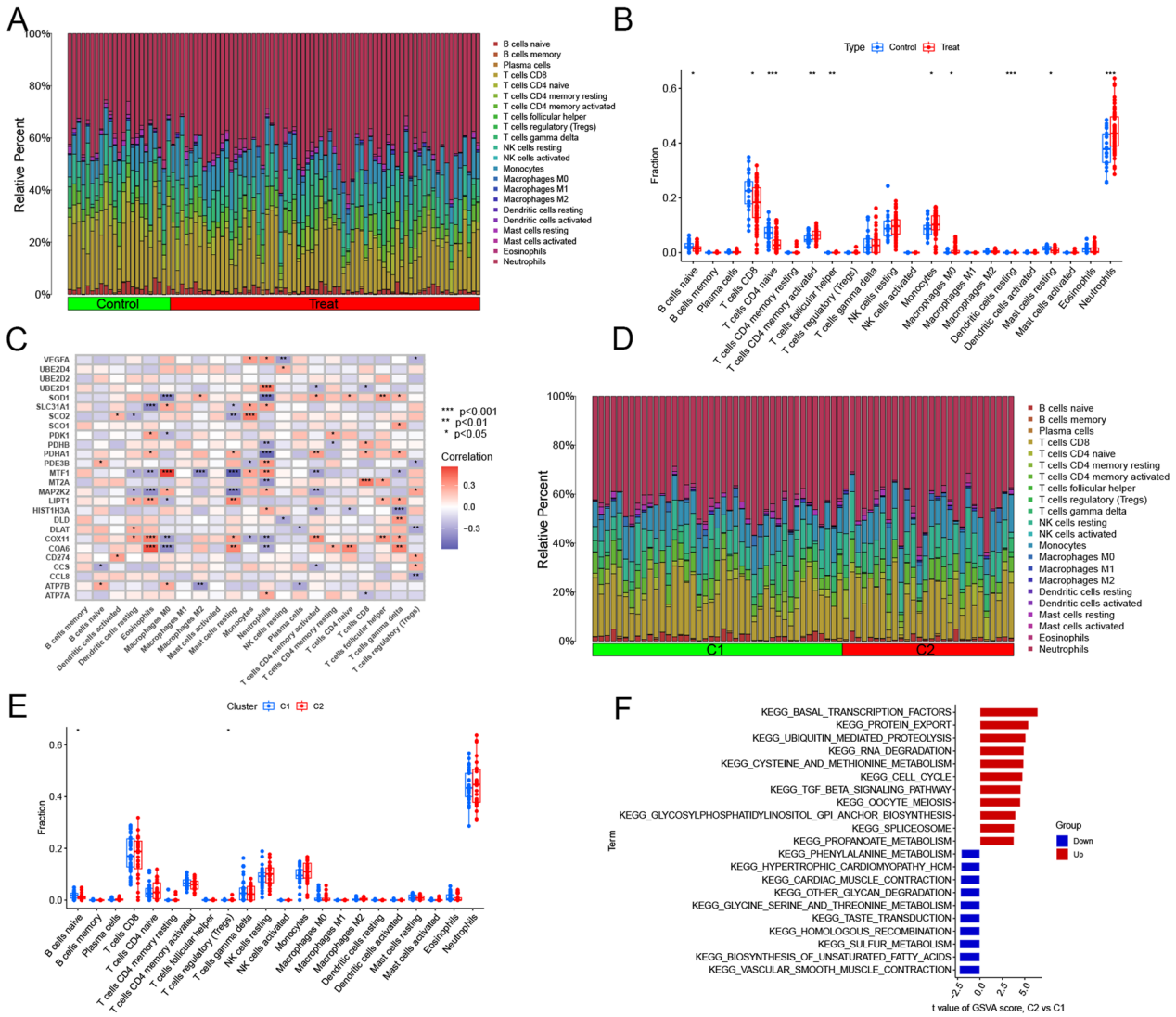

Fig. 7 The immune infiltration characteristics in AIS. **A** The relative percentage of immune infiltrating cells in each sample. **B** Boxplot showing the comparative abundance of 22 immune infiltrating cells between AIS samples and normal controls. **C** Spearman correlation analysis between the immune infiltrating cells and DECuRGs. **D** The relative proportions of immune infiltrated cells in the two clusters. **E** Discrepancies in the proportions of immune infiltrating cells among the two groups were shown in the bar graph. **F** Variations in bio-pathways between the two clusters ranked by the t-value of GSVA scores

AIS patients. The overlapping DEcircRNAs, DEmiRNAs, and DEmRNAs were identified from three independent datasets, while a circRNA-mediated ceRNA network was constructed using bioinformatics. Furthermore, we screened 26 dysregulated CuRGs from the list of DEmRNAs, suggesting a pivotal role of CuRGs in the development of AIS. We then discovered significant synergistic or antagonistic effects of most DECuRGs, as evidenced by the interactions. The immune cell abundance was also altered between controls and AIS patients. AIS samples presented elevated infiltration levels of neutrophils, M0 macrophages, activated memory $CD4^+$ T cells, follicular helper T cells, monocytes, and resting dendritic cells, consistent with previous research validated in experiments [47–49]. Numerous studies have shown the engagement of cuproptosis in immunity and neuroinflammation [50–52]. Of the 26 DECuRGs, *MTF1* was most closely correlated with the immune infiltrating cells. M0 macrophages and *MTF1* showed the most potent synergistic effects, while resting mast cells and *MTF1* presented the greatest antagonistic effect. Depending on the activation status of macrophages (M1/M2), they could have a dual role in the tissue damage process of AIS [53]. M2 macrophages contribute to neuronal regeneration

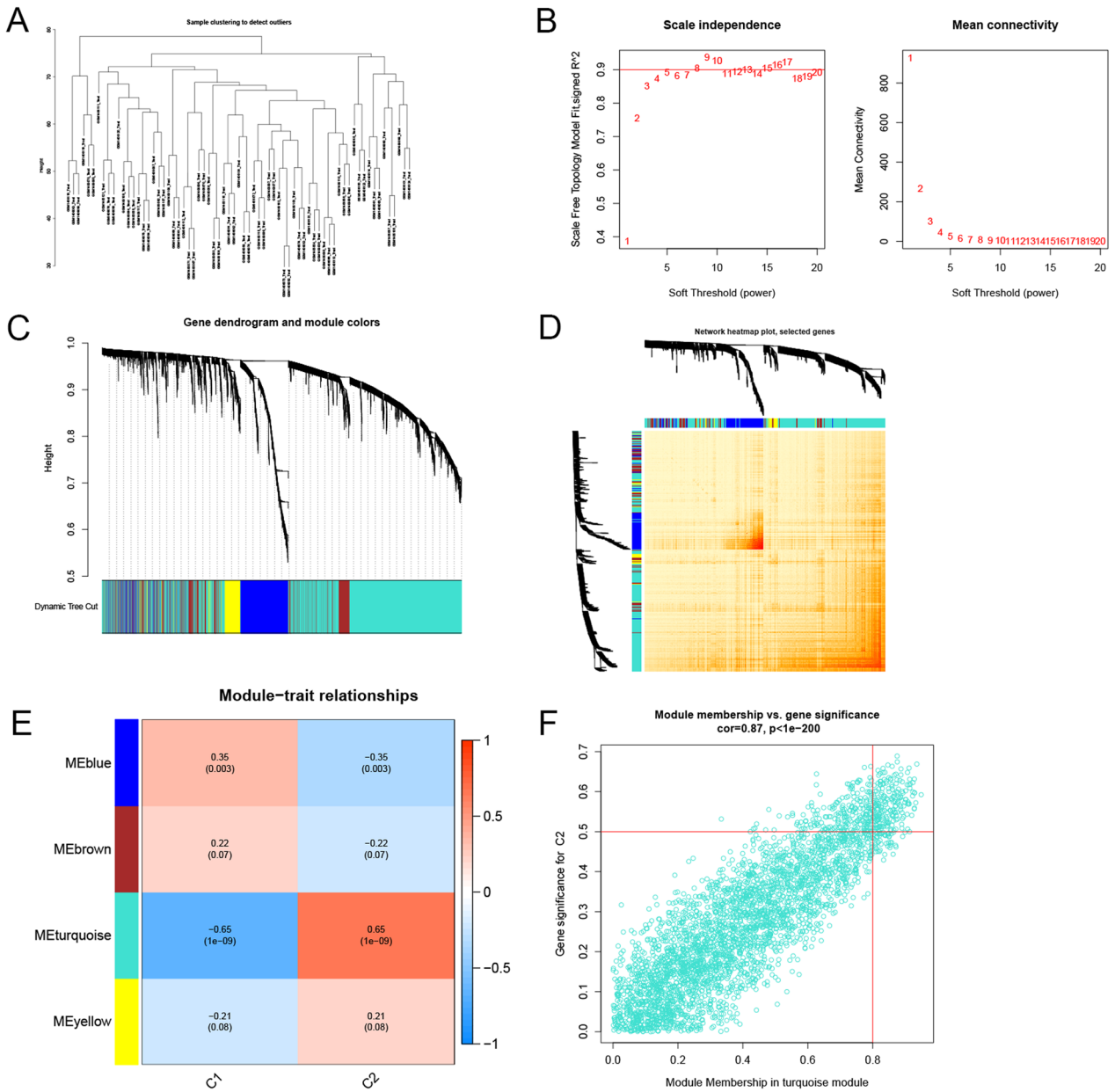

Fig. 8 **A** Clustering tree drawn using the WGCNA algorithm; the y-axis indicates the clustering distance; each branch represents a sample. **B** Analysis of the most suitable soft power. **C** Gene dendrogram with the soft threshold and four modules. **D** Network heatmap plot of the four merged modules. **E** Module-trait relationships, with the turquoise module showing the highest association. **F** Scatter plot of module members (MM) versus gene importance (GS) within the turquoise module (cor = 0.87, $p < 1e-200$)

and repair, whereas M1 macrophages are thought to have destructive properties on neurons [54]. In contrast, mast cells are reportedly involved in collateral formation and arteriogenesis in AIS [55]. Furthermore, we speculated that the cuproptosis-related ceRNA axis, *MTF1*-miR-765-circ_0040760/0068531, was associated with regulating the neuroinflammation in AIS. Both circ_0040760 and circ_0068531 act as molecular sponges of miR-765 and compete for binding with the upregulated *MTF1*. MiR-765 was reported to be implicated in inhibiting lipid metabolism in foam cell formation and oxidized LDL-macrophage models [56]. Bima et al. identified the potential of miR-765 as a reverse blood biomarker for obesity [57]. Interestingly, high-throughput screening revealed that miR-765 might serve as a PCSK9 inhibitor, leading to lower plasma LDL cholesterol levels and prevention of

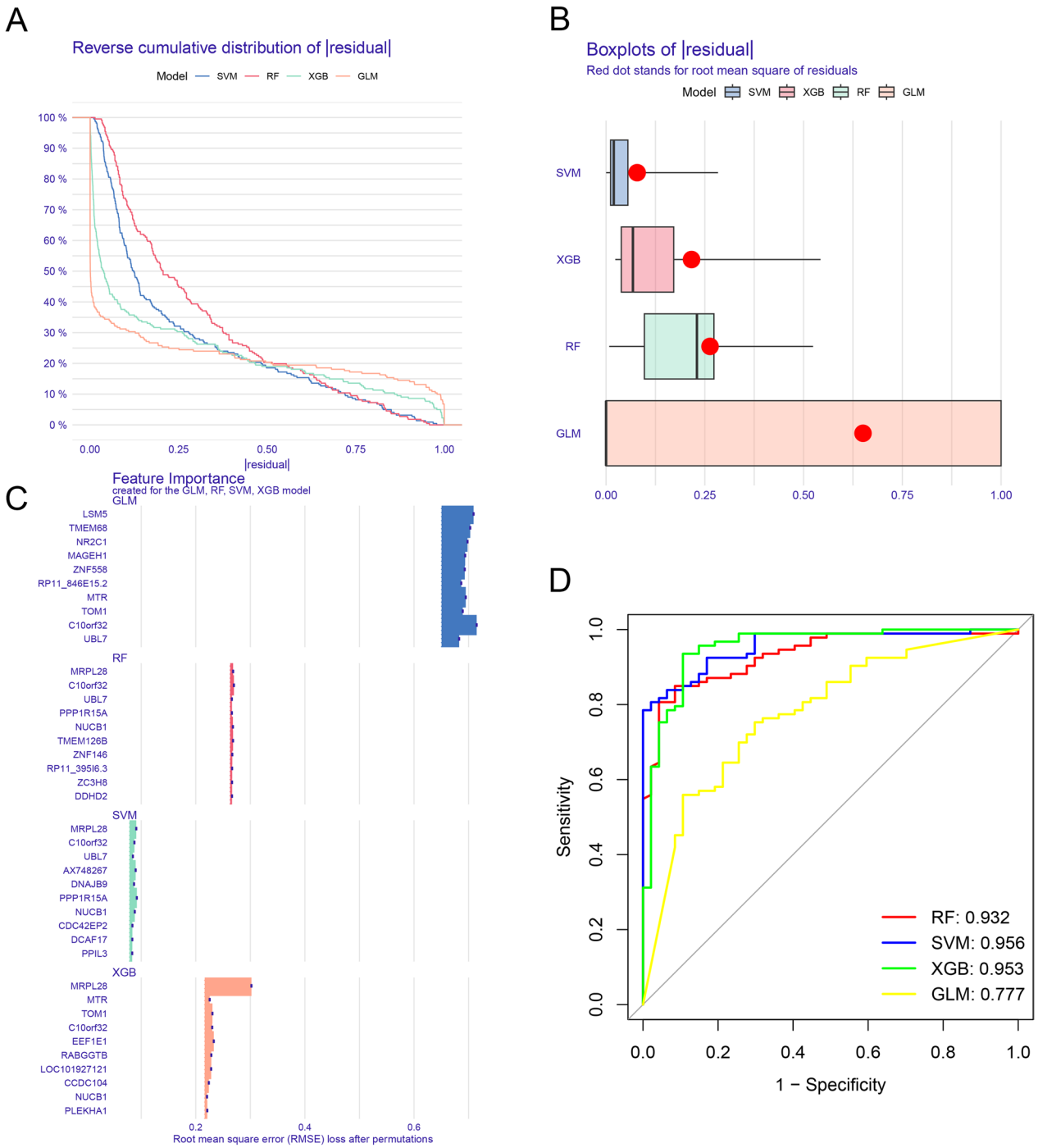

Fig. 9 Comparison of the four machine learning techniques. **A** Inverse cumulative distribution of residuals in the four models. **B** Bar graph of residuals. **C** The feature importance created for the four models. **D** The ROC curves based on fivefold cross-validation in the test cohort

cardiovascular disease [58]. In mouse models, *MTF1* was found to play a vital role in the maintenance and induction of inflammatory pain [59]. There were few reports on hsa_circ_0040760 and hsa_circ_0068531. Unfortunately, the expression matrix of miRNAs in AIS was rarely seen in the GEO database. Therefore, further studies are required to confirm and explore our findings.

In the enrichment analyses, we applied three different methods to explore the biological functions. We found the 26 DECuRGs in AIS were primarily enriched in the

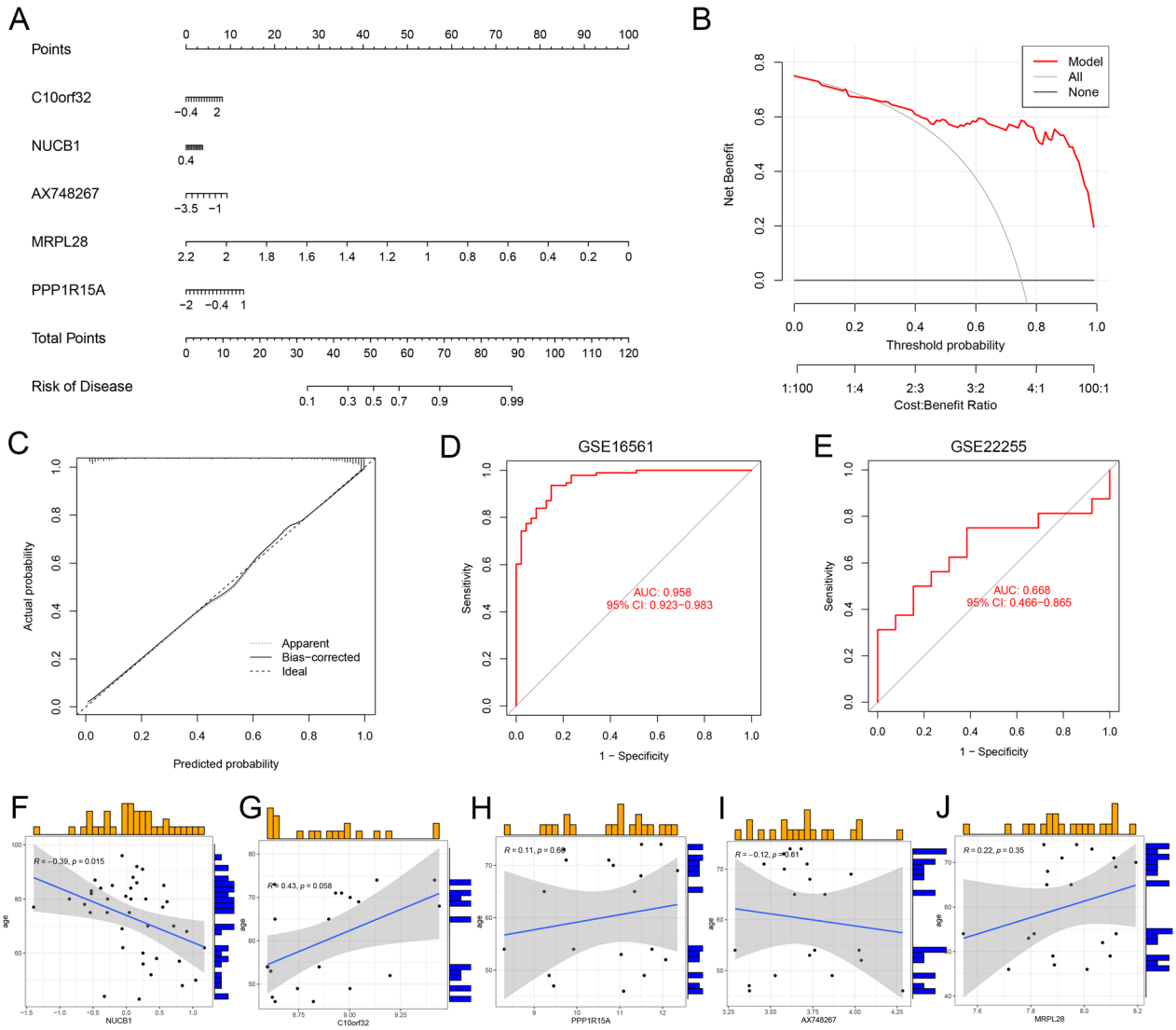

Fig. 10 Establishment and validation of the risk model. **A** Construction of the nomogram with the top 5 most significant variables. Establishment of the DCA (**B**) and calibration curves (**C**) to evaluate the efficiency of the nomogram. **D**, **E** External validation via the ROC curves analysis (**F**–**J**)

cellular response to stimuli, copper homeostasis, and regulation of pyruvate dehydrogenase, which have been reported in previous studies regarding the immune regulation of AIS [60–62]. The top 5 most enriched pathways of DECuRGs were the HIF-1 signaling pathway, central carbon metabolism in cancer, pyruvate metabolism, TCA cycle, and glycolysis. The findings suggest that the genes are particularly associated not only with the relevant cuproptosis-related pathways but are also engaged in other biological mechanisms, such as immune responses and oxidative stress [63–65]. This demonstrates that these DECuRGs serve distinct functions in specific environments. There may be cross-talk between these biopathways, consistent with previous reports revealing a significant interaction between cuproptosis and immune responses [50, 66]. In addition, we conducted a hub locus analysis to determine key nodes and found that *MTF1* was also the core node of the cuproptosis-related regulatory network. The gene *MTF1* is an essential hypoxia-sensitive transcription factor that might function in the neuroprotective effects mediated by remote limb ischemic postconditioning via activation of NCX1 [67]. Moreover, Youn et al. [68] found that enhanced MTF1 expression may help protect against cerebral ischemia, and hypothermia was an inductor of MT gene expression in brain endothelial cells. In mouse models of focal cerebral ischemia, sevoflurane conferred neuroprotection by activating NO and peroxides to increase MT-1 and MT-2

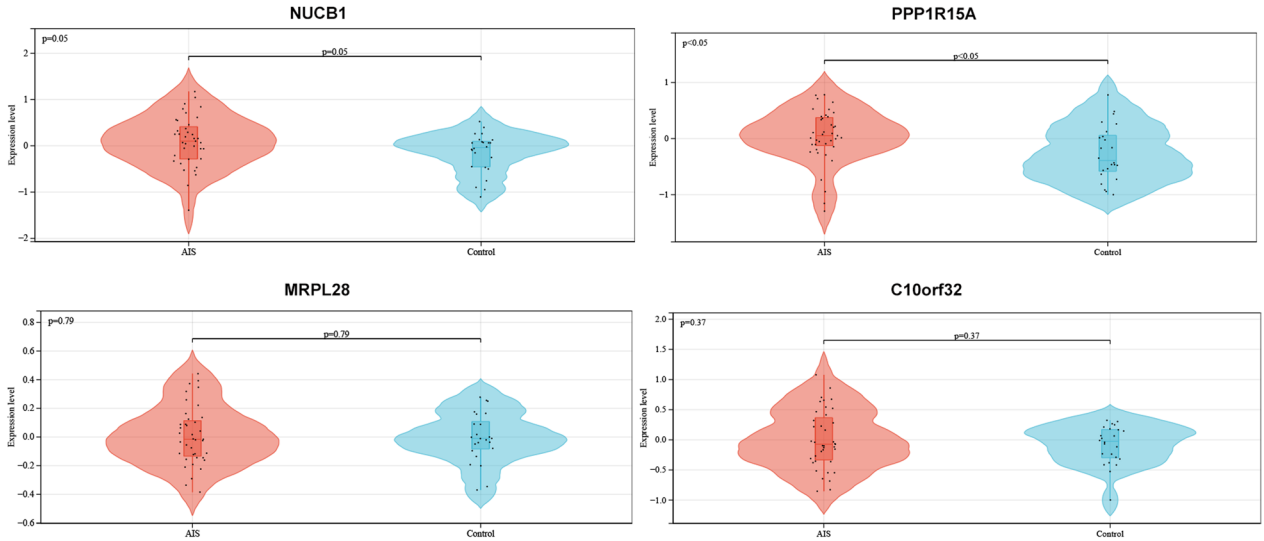

Fig. 11 The expression of these four genes differed between AIS samples and normal controls. Of these, *NUCB1* and *PPP1R15A* were considered statistically significant

expression and enhance the expression of MTF-1 in the nucleus [69]. All these findings are consistent with our results.

Based on the expression patterns of key nodes, we identified two distinct cuproptosis-related molecular groups in AIS patients. The expression levels of *MTF1* were not significantly different between the two clusters. Cluster 1 displayed higher levels of the critical DECuRGs abundance. GSVA analysis showed that Cluster1 was mainly enriched in the vascular smooth muscle contraction, biosynthesis of unsaturated fatty acids, and sulfur metabolism, while basal transcription factors and protein export characterized Cluster2. Combined with the immune infiltration analysis, we concluded that though the biological processes differed between the two cuproptosis-related groups, the intrinsic immune environment was not significantly altered, possibly due to the small numbers of AIS samples. Therefore, further research is necessary to verify this finding.

Recently, machine learning techniques based on high-precision imaging metrics and demographic methods have been increasingly employed to construct risk models in cerebrovascular diseases [70–72]. Several machine-learning methods have been proposed for merging spatial transcriptome data with other data [73]. In this work, we first screened out the most significant module consisting of 254 hub genes using the WGCNA algorithm. We comprehensively assessed the performance of four machine learning methods. We developed an SVM-based model with the highest area under the curves (AUC = 0.956), indicating the satisfactory ability of this model to predict AIS risk. Afterward, we selected the top 5 most important variables (*C10orf32*, *NUCB1*, *AX748267*, *MRPL28*, and *PPP1R15A*) to construct a nomogram model. The DCA calibration curves demonstrated the independence of this 5-gene signature and ROC analysis (AUC = 0.958 and 0.668). The AUC value of the GSE22255 dataset was relatively lower. One plausible explanation could be that the experiment was performed in peripheral blood mononuclear cells, not whole blood.

Furthermore, we validated the five hub genes using the GSE16561 dataset. We found that only *PPP1R15A* and *NUCB1* were statistically upregulated in the AIS samples, consistent with our results. This could be associated with the small sample size of this dataset. The autophagy gene *PPP1R15A* was reported to be markedly related to immune response activity in ischemic stroke [74]. Lelong et al. observed a strong early upregulation of *PPP1R15A* expression in the novel mouse models of monocular amaurosis fugax, which will help test novel neuroprotective drugs [75]. Nucleobindin 1 (*NUCB1*) is a clearly defined Golgi protein whose function is related to G-protein signaling, immunity, and calcium homeostasis [76]. Studies have revealed that nestin-1-like peptides encoded by *NUCB1* exert a protective role after cardiac muscle injury and also defend dopaminergic cells from neurotoxicity through anti-apoptotic and anti-inflammatory mechanisms [77]. In the brain ischemia/reperfusion models of Wistar rats, nesfatin-1 had remarkable neuroprotective effects through inhibition of caspase-3 and microglia activation [78]. Age is the most influential non-interventional risk factor for AIS, and the incidence of AIS increases sharply with age. Among the five predictor genes, we

found that only *NUCB1* was adversely correlated with age (R = −0.39, $p = 0.015$). Overall, this risk model was a promising indicator for evaluating AD subgroups and incidence risk.

To our knowledge, this study presented the first cuproptosis-involved model for AIS. However, there were still some limitations that should be admitted. Firstly, the cuproptosis-related genes enrolled in the study were primarily from prior research, and thus, many potential genes may have been excluded or omitted. Second, the gene expression profiling of selected datasets was tested under different conditions in different laboratories, which may bias the results. Third, the identified cuproptosis-related ceRNA network and risk model required further experimental studies. One more major limitation was the lack of prospective AIS cohorts to verify the model's stratification performance and risk role.

Conclusion

In summary, this study suggested that these cuproptosis-related genes and their interactions may be involved in the development of AIS. The key nodes and *MTF1*-miR-765-circ_0040760/ 0068531 axis determined in this study may serve essential roles in regulating the above processes. We identified five hub genes, specifically *PPP1R15A* and *NUCB1*, as diagnostic features for identifying AIS. These findings may offer novel insights into the diagnosis and treatment of AIS.

Supplementary Information

The online version contains supplementary material available at https://doi.org/10.1186/s43042-023-00457-3.

Additional file 1. The 46 cuproptosis-related genes screened from other studies.

Additional file 2. The top enriched GO terms of the DECuRGs.

Additional file 3. The KEGG terms of the DECuRGs.

Additional file 4. The 254 hub genes related to AIS in the turquoise module.

Additional file 5. **Figure S1**: The expression levels of key nodes in different tissues. The critical genes MTF1 (A), MIR765 (B), UBE2D2 (C), and MIR4679 (D) results in the GeneCards database. Green represents the expression levels in nerve tissues; red denotes the expression levels in immune tissues.

Additional file 6. **Figure S2**: Bulk tissue gene expressions for MTF1 (A), MIR765 (B), UBE2D2 (C), and MIR4679 (D) in the GTEx database.

Acknowledgements
We appreciate all the researchers and institutions who provided data for this study.

Author contributions
JF and BZ participated in manuscript writing and data analysis. CL and WY contributed to the revision of the manuscript. ZL and ZW designed and supervised the study. All authors have read and approved the final draft.

Funding
This study was supported by the National Natural Science Foundation of China (82072777), Natural Science Foundation of Fujian Province (2020J02063), the Fujian Provincial Clinical Research Center for Brain Diseases (2021FJSLCYX01), Fujian Province Health Commission (2022GGB010), and Xiamen Municipal Bureau of Science and Technology (3502Z20209005).

Availability of data and materials
The datasets supporting the current study results are available in the GEO database (https://www.ncbi.nlm.nih.gov/geo), further queries can be directed to the corresponding author.

Declarations

Ethics approval and consent to participate
Ethics committee approval and patient consent were not required to conduct this study as the datasets were from public databases.

Consent for publication
Not applicable.

Competing interests
No competing interests.

Author details
[1]Department of Neurosurgery, Xiamen Key Laboratory of Brain Center, the First Affiliated Hospital of Xiamen University, School of Medicine, Xiamen University, Xiamen, China.

Received: 24 July 2023 Accepted: 24 November 2023
Published online: 29 November 2023

References

1. Abbafati C, Abbas KM, Abbasi M, Abbasifard M, Abbasi-Kangevari M, Abbastabar H et al (2020) Global burden of 369 diseases and injuries in 204 countries and territories, 1990–2019: a systematic analysis for the Global Burden of Disease Study 2019. Lancet 396(10258):1204–1222
2. Jian Z, Liu R, Zhu X, Smerin D, Zhong Y, Gu L et al (2019) The involvement and therapy target of immune cells after ischemic stroke. Front Immunol 10:2167
3. Yang C, Hawkins KE, Doré S, Candelario-Jalil E (2019) Neuroinflammatory mechanisms of blood–brain barrier damage in ischemic stroke. Am J Physiol Cell Physiol 316(2):C135–C153
4. Ma H, Jiang Z, Xu J, Liu J, Guo ZN (2021) Targeted nano-delivery strategies for facilitating thrombolysis treatment in ischemic stroke. Drug Deliv 28(1):357–371
5. Li Y (2020) Copper homeostasis: emerging target for cancer treatment. IUBMB Life 72(9):1900–1908
6. Alfaidy N, Chauvet S, Donadio-Andrei S, Salomon A, Saoudi Y, Richaud P et al (2013) Prion protein expression and functional importance in developmental angiogenesis: role in oxidative stress and copper homeostasis. Antioxid Redox Signal 18(4):400–411
7. Valko M, Jomova K, Rhodes CJ, Kuča K, Musílek K (2016) Redox- and non-redox-metal-induced formation of free radicals and their role in human disease. Arch Toxicol 90(1):1–37
8. Tsvetkov P, Coy S, Petrova B, Dreishpoon M, Verma A, Abdusamad M et al (2022) Copper induces cell death by targeting lipoylated TCA cycle proteins. Science 375(6586):1254–1261
9. Oliveri V (2022) Selective targeting of cancer cells by copper ionophores: an overview. Front Mol Biosci 9:841814
10. Peng F, Muzik O, Gatson J, Kernie SG, Diaz-Arrastia R (2015) Assessment of traumatic brain injury by increased 64Cu uptake on 64CuCl2 PET/CT. J Nucl Med 56(8):1252–1257
11. Mangalmurti A, Lukens JR (2022) How neurons die in Alzheimer's disease: implications for neuroinflammation. Curr Opin Neurobiol 75:102575

12. Chelly J, Tümer Z, Tønnesen T, Petterson A, Ishikawa-Brush Y, Tommerup N et al (1993) Isolation of a candidate gene for Menkes disease that encodes a potential heavy metal binding protein. Nat Genet 3(1):14–19
13. Jiang Y, Wang LP, Dong XH, Cai J, Jiang GJ, Zhang C et al (2015) Trace amounts of copper in drinking water aggravate cerebral ischemic injury via impairing endothelial progenitor cells in mice. CNS Neurosci Ther 21(8):677–680
14. An Y, Li S, Huang X, Chen X, Shan H, Zhang M (2022) The role of copper homeostasis in brain disease. Int J Mol Sci 23(22)
15. Huuskonen MT, Tuo QZ, Loppi S, Dhungana H, Korhonen P, McInnes LE et al (2017) The copper bis(thiosemicarbazone) complex Cu(II)(atsm) Is protective against cerebral ischemia through modulation of the inflammatory milieu. Neurotherapeutics 14(2):519–532
16. Mirończuk A, Kapica-Topczewska K, Socha K, Soroczyńska J, Jamiołkowski J, Kułakowska A, et al (2021) Selenium, copper, zinc concentrations and Cu/Zn, Cu/Se molar ratios in the serum of patients with acute ischemic stroke in Northeastern Poland-A new insight into stroke pathophysiology. Nutrients 13(7)
17. Li J, Wang J, Wang Z (2021) Circ_0006768 upregulation attenuates oxygen-glucose deprivation/reoxygenation-induced human brain microvascular endothelial cell injuries by upregulating VEZF1 via miR-222-3p inhibition. Metab Brain Dis 36(8):2521–2534
18. Ding MH, Lozoya EG, Rico RN, Chew SA (2020) The role of angiogenesis-inducing microRNAs in vascular tissue engineering. Tissue Eng Part A 26(23–24):1283–1302
19. Yang L, Han B, Zhang Z, Wang S, Bai Y, Zhang Y et al (2020) Extracellular vesicle-mediated delivery of circular RNA SCMH1 promotes functional recovery in rodent and nonhuman primate ischemic stroke models. Circulation 142(6):556–574
20. Chen G, Shan X, Li L, Dong L, Huang G, Tao H (2022) circHIPK3 regulates apoptosis and mitochondrial dysfunction induced by ischemic stroke in mice by sponging miR-148b-3p via CDK5R1/SIRT1. Exp Neurol 355:114115
21. Zhao H, Han Z, Ji X, Luo Y (2016) Epigenetic regulation of oxidative stress in ischemic stroke. Aging Dis 7(3):295–306
22. Kunze R, Fischer S, Marti HH, Preissner KT (2023) Brain alarm by self-extracellular nucleic acids: from neuroinflammation to neurodegeneration. J Biomed Sci 30(1):64
23. Ritchie ME, Phipson B, Wu D, Hu Y, Law CW, Shi W, et al (2015) limma powers differential expression analyses for RNA-sequencing and microarray studies. Nucleic Acids Res 43(7)
24. Leek JT (2014) svaseq: removing batch effects and other unwanted noise from sequencing data. Nucleic Acids Res 42(21)
25. Abrahamsson TR, Jakobsson HE, Andersson AF, Bjorksten B, Engstrand L, Jenmalm MC (2012) Low diversity of the gut microbiota in infants with atopic eczema. J Allergy Clin Immunol 129(2):434-U244
26. Schober P, Boer C, Schwarte LA (2018) Correlation coefficients: appropriate use and interpretation. Anesth Analg 126(5):1763–1768
27. Fishilevich S, Zimmerman S, Kohn A, Iny Stein T, Olender T, Kolker E, et al (2016) Genic insights from integrated human proteomics in GeneCards. Database 2016
28. Safran M, Dalah I, Alexander J, Rosen N, Iny Stein T, Shmoish M, et al (2010) GeneCards Version 3: the human gene integrator. Database (Oxford). 2010:baq020
29. Zhou Y, Zhou B, Pache L, Chang M, Khodabakhshi AH, Tanaseichuk O, et al (2019) Metascape provides a biologist-oriented resource for the analysis of systems-level datasets. Nat Commun 10
30. Kanehisa M, Sato Y, Kawashima M (2022) KEGG mapping tools for uncovering hidden features in biological data. Protein Sci 31(1):47–53
31. Dudekulay DB, Panda AC, Grammatikakis I, De S, Abdelmohsen K, Gorospe M (2016) CircInteractome: a web tool for exploring circular RNAs and their interacting proteins and microRNAs. RNA Biol 13(1):34–42
32. Wilkerson MD, Hayes DN (2010) ConsensusClusterPlus: a class discovery tool with confidence assessments and item tracking. Bioinformatics 26(12):1572–1573
33. Newman AM, Liu CL, Green MR, Gentles AJ, Feng W, Xu Y et al (2015) Robust enumeration of cell subsets from tissue expression profiles. Nat Methods 12(5):453
34. Wan Q, Tang J, Han Y, Wang D (2018) Co-expression modules construction by WGCNA and identify potential prognostic markers of uveal melanoma. Exp Eye Res 166:13–20
35. Fernandez-Delgado M, Cernadas E, Barro S, Amorim D (2014) Do we Need hundreds of classifiers to solve real world classification problems? J Mach Learn Res 15:3133–3181
36. Venerito V, Angelini O, Fornaro M, Cacciapaglia F, Lopalco G, Iannone F (2022) A machine learning approach for predicting sustained remission in rheumatoid arthritis patients on biologic agents. JCR-J Clin Rheumatol 28(2):E334–E339
37. Shah AD, Bartlett JW, Carpenter J, Nicholas O, Hemingway H (2014) Comparison of random forest and parametric imputation models for imputing missing data using MICE: a CALIBER study. Am J Epidemiol 179(6):764–774
38. Huang S, Cai N, Pacheco PP, Narandes S, Wang Y, Xu W (2018) Applications of support vector machine (SVM) learning in cancer genomics. Cancer Genomics Proteomics 15(1):41–51
39. Winkler AM, Ridgway GR, Webster MA, Smith SM, Nichols TE (2014) Permutation inference for the general linear model. Neuroimage 92:381–397
40. Li Y, Ma T, Zhu X, Zhang M, Zhao L, Wang P et al (2022) Zinc improves neurological recovery by promoting angiogenesis via the astrocyte-mediated HIF-1α/VEGF signaling pathway in experimental stroke. CNS Neurosci Ther 28(11):1790–1799
41. Chen X, Cai Q, Liang R, Zhang D, Liu X, Zhang M et al (2023) Copper homeostasis and copper-induced cell death in the pathogenesis of cardiovascular disease and therapeutic strategies. Cell Death Dis 14(2):105
42. Sakata H, Niizuma K, Wakai T, Narasimhan P, Maier CM, Chan PH (2012) Neural stem cells genetically modified to overexpress Cu/Zn-superoxide dismutase enhance amelioration of ischemic stroke in mice. Stroke 43(9):2423
43. Adamsson Eryd S, Smith JG, Melander O, Hedblad B, Engström G (2011) Inflammation-sensitive proteins and risk of atrial fibrillation: a population-based cohort study. Eur J Epidemiol 26(6):449–455
44. Zhang S, Song G, Yuan J, Qiao S, Xu S, Si Z, et al (2020) Circular RNA circ_0003204 inhibits proliferation, migration and tube formation of endothelial cell in atherosclerosis via miR-370-3p/TGF beta R2/phosph-SMAD3 axis. J Biomed Sci 27(1)
45. Karreth FA, Pandolfi PP (2013) ceRNA cross-talk in cancer: when ce-bling rivalries go awry. Cancer Discov 3(10):1113–1121
46. Bu X, Zhao Y, Chang M, Ge X (2021) Downregulation of lncRNA SNHG14 alleviates neurons injury by modulating the miR-181c-5p/BMF axis in ischemic stroke. Brain Res Bull 174:379–388
47. Jickling GC, Liu D, Ander BP, Stamova B, Zhan X, Sharp FR (2015) Targeting neutrophils in ischemic stroke: translational insights from experimental studies. J Cereb Blood Flow Metab 35(6):888–901
48. Sinha RK, Flynn R, Zaiken M, Paz K, Gavin AL, Nemazee D et al (2019) Activated protein C ameliorates chronic graft-versus-host disease by PAR1-dependent biased cell signaling on T cells. Blood 134(9):776–781
49. Lee GA, Lin T-N, Chen C-Y, Mau S-Y, Huang W-Z, Kao Y-C et al (2018) Interleukin 15 blockade protects the brain from cerebral ischemia-reperfusion injury. Brain Behav Immun 73:562–570
50. Cai Z, He Ye, Yu Z, Hu J, Xiao Z, Zu X, et al (2022) Cuproptosis-related modification patterns depict the tumor microenvironment, precision immunotherapy, and prognosis of kidney renal clear cell carcinoma. Front Immunol 13
51. Chen B, Zhou X, Yang L, Zhou H, Meng M, Zhang L, et al (2022) A cuproptosis activation scoring model predicts neoplasm-immunity interactions and personalized treatments in glioma. Comput Biol Med 148
52. Wang Y, Zhang X, Chen Y, Zhu B, Xing Q (2022) Identification of hub biomarkers and exploring the roles of immunity, M6A, ferroptosis, or cuproptosis in rats with diabetic erectile dysfunction. Andrology
53. Hu X, Li P, Guo Y, Wang H, Leak RK, Chen S et al (2012) Microglia/macrophage polarization dynamics reveal novel mechanism of injury expansion after focal cerebral ischemia. Stroke 43(11):3063-U474
54. Vogel DYS, Heijnen PDAM, Breur M, de Vries HE, Tool ATJ, Amor S, et al (2014) Macrophages migrate in an activation-dependent manner to chemokines involved in neuroinflammation. J Neuroinflam 11
55. Bot I, van der Velden D, Bouwman M, Kroner MJ, Kuiper J, Quax PHA, et al (2020) Local mast cell activation promotes neovascularization. Cells 9(3)
56. Ye B, Liang X, Zhao Y, Cai X, Wang Z, Lin S, et al (2022) Research paper Hsa_circ_0007478 aggravates NLRP3 inflammasome activation and lipid metabolism imbalance in ox-LDL-stimulated macrophage via miR-765/EFNA3 axis. Chemico-Biol Interact 368

57. Bima AI, Elsamanoudy AZ, Alamri AS, Felimban R, Felemban M, Alghamdi KS et al (2022) Integrative global co-expression analysis identifies key microRNA-target gene networks as key blood biomarkers for obesity. Minerva Med 113(3):532–41
58. van Solingen C, Oldebeken SR, Salerno AG, Wanschel A, Moore KJ (2021) High-throughput screening identifies MicroRNAs regulating human PCSK9 and hepatic low-density lipoprotein receptor expression. Front Cardiovasc Med 8:667298
59. Hao L-Y, Zhang M, Tao Y, Xu H, Liu Q, Yang K, et al (2022) miRNA-22 Upregulates Mtf1 in Dorsal horn neurons and is essential for inflammatory pain. Oxidative Medicine and Cellular Longevity. 2022
60. Kuramshina DB, Novikova LB, Nikonov AA, Torshin IY, Gromova OA (2012) Analysis of a disturbance of trace element balance in patients with ischemic stroke with arterial hypertension. Zhurnal Nevrologii I Psikhiatrii Imeni S S Korsakova 112(3):42–6
61. Becker K (2012) Autoimmune responses to brain following stroke. Transl Stroke Res 3(3):310–7
62. Cai L, Thibodeau A, Peng C, Ji X, Rastogi R, Xin R et al (2016) Combination therapy of normobaric oxygen with hypothermia or ethanol modulates pyruvate dehydrogenase complex in thromboembolic cerebral ischemia. J Neurosci Res 94(8):749–58
63. Pan T, Sun S, Chen Y, Tian R, Chen E, Tan R et al (2022) Immune effects of PI3K/Akt/HIF-1α-regulated glycolysis in polymorphonuclear neutrophils during sepsis. Crit Care 26(1):29
64. Xia H, Huang Z, Xu Y, Yam JWP, Cui Y (2022) Reprogramming of central carbon metabolism in hepatocellular carcinoma. Biomed Pharmacother 153:113485
65. Chen L, Min J, Wang F (2022) Copper homeostasis and cuproptosis in health and disease. Signal Transduct Target Ther 7(1):378
66. Song S, Zhang M, Xie P, Wang S, Wang Y (2022) Comprehensive analysis of cuproptosis-related genes and tumor microenvironment infiltration characterization in breast cancer. Front Immunol 13
67. Valsecchi V, Laudati G, Cuomo O, Sirabella R, Annunziato L, Pignataro G (2021) The hypoxia sensitive metal transcription factor MTF-1 activates NCX1 brain promoter and participates in remote postconditioning neuroprotection in stroke. Cell Death Dis 12(5):423
68. Park YH, Lee YM, Kim DS, Park J, Suk K, Kim JK et al (2013) Hypothermia enhances induction of protective protein metallothionein under ischemia. J Neuroinflammation 10:21
69. Liu J, Tan S, Wang Y, Luo J, Long Y, Mei X et al (2020) Role of metallothionein-1 and metallothionein-2 in the neuroprotective mechanism of sevoflurane preconditioning in mice. J Mol Neurosci 70(5):713–23
70. Wang J, Kang Z, Liu Y, Li Z, Liu Y, Liu J (2022) Identification of immune cell infiltration and diagnostic biomarkers in unstable atherosclerotic plaques by integrated bioinformatics analysis and machine learning. Front Immunol 13:956078
71. Heo J, Yoon JG, Park H, Kim YD, Nam HS, Heo JH (2019) Machine learning-based model for prediction of outcomes in acute stroke. Stroke 50(5):1263–5
72. Murray NM, Unberath M, Hager GD, Hui FK (2020) Artificial intelligence to diagnose ischemic stroke and identify large vessel occlusions: a systematic review. J Neurointerv Surg 12(2):156–64
73. Zeng Z, Li Y, Li Y, Luo Y (2022) Statistical and machine learning methods for spatially resolved transcriptomics data analysis. Genome Biol 23(1):83
74. Li S, Zhang Y, Shi SS, Guo D, Chang T (2022) Identification of immune characteristic landscapes related to autophagy in ischemic stroke. Front Cell Dev Biol 10
75. Lelong DC, Bieche I, Perez E, Bigot K, Leemput J, Laurendeau I et al (2007) Novel mouse model of monocular amaurosis fugax. Stroke 38(12):3237–44
76. Gonzalez R, Mohan H, Unniappan S (2012) Nucleobindins: Bioactive precursor proteins encoding putative endocrine factors? Gen Comp Endocrinol 176(3):341–6
77. Su R-Y, Geng X-Y, Yang Y, Yin H-S (2021) Nesfatin-1 inhibits myocardial ischaemia/reperfusion injury through activating Akt/ERK pathway-dependent attenuation of endoplasmic reticulum stress. J Cell Mol Med 25(11):5050–9
78. Erfani S, Moghimi A, Aboutaleb N, Khaksari M (2018) Nesfatin-1 improve spatial memory impairment following transient global cerebral ischemia/reperfusion via inhibiting microglial and caspase-3 activation. J Mol Neurosci 65(3):377–84

Publisher's Note